

**Flow Measurements via Two-particle Azimuthal Correlations
in Au + Au Collisions at $\sqrt{s_{NN}} = 130$ GeV.**

K. Adcox,⁴⁰ S. S. Adler,³ N. N. Ajitanand,²⁷ Y. Akiba,¹⁴ J. Alexander,²⁷ L. Aphecetche,³⁴ Y. Arai,¹⁴ S. H. Aronson,³ R. Averbeck,²⁸ T. C. Awes,²⁹ K. N. Barish,⁵ P. D. Barnes,¹⁹ J. Barrette,²¹ B. Bassalleck,²⁵ S. Bathe,²² V. Baublis,³⁰ A. Bazilevsky,^{12,32} S. Belikov,^{12,13} F. G. Bellaiche,²⁹ S. T. Belyaev,¹⁶ M. J. Bennett,¹⁹ Y. Berdnikov,³⁵ S. Botelho,³³ M. L. Brooks,¹⁹ D. S. Brown,²⁶ N. Bruner,²⁵ D. Bucher,²² H. Buesching,²² V. Bumazhnov,¹² G. Bunce,^{3,32} J. Burward-Hoy,²⁸ S. Butsyk,^{28,30} T. A. Carey,¹⁹ P. Chand,² J. Chang,⁵ W. C. Chang,¹ L. L. Chavez,²⁵ S. Chernichenko,¹² C. Y. Chi,⁸ J. Chiba,¹⁴ M. Chiu,⁸ R. K. Choudhury,² T. Christ,²⁸ T. Chujo,^{3,39} M. S. Chung,^{15,19} P. Chung,²⁷ V. Cianciolo,²⁹ B. A. Cole,⁸ D. G. D'Enterria,³⁴ G. David,³ H. Delagrangé,³⁴ A. Denisov,¹² A. Deshpande,³² E. J. Desmond,³ O. Dietzsch,³³ B. V. Dinesh,² A. Drees,²⁸ A. Durum,¹² D. Dutta,² K. Ebisu,²⁴ Y. V. Efremenko,²⁹ K. El Chenawi,⁴⁰ H. En'yo,^{17,31} S. Esumi,³⁹ L. Ewell,³ T. Ferdousi,⁵ D. E. Fields,²⁵ S. L. Fokin,¹⁶ Z. Fraenkel,⁴² A. Franz,³ A. D. Frawley,⁹ S.-Y. Fung,⁵ S. Garpman,²⁰ T. K. Ghosh,⁴⁰ A. Glenn,³⁶ A. L. Godoi,³³ Y. Goto,³² S. V. Greene,⁴⁰ M. Grosse Perdekamp,³² S. K. Gupta,² W. Guryn,³ H.-Å. Gustafsson,²⁰ J. S. Haggerty,³ H. Hamagaki,⁷ A. G. Hansen,¹⁹ H. Hara,²⁴ E. P. Hartouni,¹⁸ R. Hayano,³⁸ N. Hayashi,³¹ X. He,¹⁰ T. K. Hemmick,²⁸ J. M. Heuser,²⁸ M. Hibino,⁴¹ J. C. Hill,¹³ D. S. Ho,⁴³ K. Homma,¹¹ B. Hong,¹⁵ A. Hoover,²⁶ T. Ichihara,^{31,32} K. Imai,^{17,31} M. S. Ippolitov,¹⁶ M. Ishihara,^{31,32} B. V. Jacak,^{28,32} W. Y. Jang,¹⁵ J. Jia,²⁸ B. M. Johnson,³ S. C. Johnson,^{18,28} K. S. Joo,²³ S. Kametani,⁴¹ J. H. Kang,⁴³ M. Kann,³⁰ S. S. Kapoor,² S. Kelly,⁸ B. Khachaturov,⁴² A. Khanzadeev,³⁰ J. Kikuchi,⁴¹ D. J. Kim,⁴³ H. J. Kim,⁴³ S. Y. Kim,⁴³ Y. G. Kim,⁴³ W. W. Kinnison,¹⁹ E. Kistenev,³ A. Kiyomichi,³⁹ C. Klein-Boesing,²² S. Klinksiek,²⁵ L. Kochenda,³⁰ V. Kochetkov,¹² D. Koehler,²⁵ T. Kohama,¹¹ D. Kotchetkov,⁵ A. Kozlov,⁴² P. J. Kroon,³ K. Kurita,^{31,32} M. J. Kweon,¹⁵ Y. Kwon,⁴³ G. S. Kyle,²⁶ R. Lacey,²⁷ J. G. Lajoie,¹³ J. Lauret,²⁷ A. Lebedev,^{13,16} D. M. Lee,¹⁹ M. J. Leitch,¹⁹ X. H. Li,⁵ Z. Li,^{6,31} D. J. Lim,⁴³ M. X. Liu,¹⁹ X. Liu,⁶ Z. Liu,⁶ C. F. Maguire,⁴⁰ J. Mahon,³ Y. I. Makdisi,³ V. I. Manko,¹⁶ Y. Mao,^{6,31} S. K. Mark,²¹ S. Markacs,⁸ G. Martinez,³⁴ M. D. Marx,²⁸ A. Masaike,¹⁷ F. Matathias,²⁸ T. Matsumoto,^{7,41} P. L. McGaughey,¹⁹ E. Melnikov,¹² M. Mersmeyer,²² F. Messer,²⁸ M. Messer,³ Y. Miake,³⁹ T. E. Miller,⁴⁰ A. Milov,⁴² S. Mioduszewski,^{3,36} R. E. Mischke,¹⁹ G. C. Mishra,¹⁰ J. T. Mitchell,³ A. K. Mohanty,² D. P. Morrison,³ J. M. Moss,¹⁹ F. Mühlbacher,²⁸ M. Muniruzzaman,⁵ J. Murata,³¹ S. Nagamiya,¹⁴ Y. Nagasaka,²⁴ J. L. Nagle,⁸ Y. Nakada,¹⁷ B. K. Nandi,⁵ J. Newby,³⁶ L. Nikkinen,²¹ P. Nilsson,²⁰ S. Nishimura,⁷ A. S. Nyanin,¹⁶ J. Nystrand,²⁰ E. O'Brien,³ C. A. Ogilvie,¹³ H. Ohnishi,^{3,11} I. D. Ojha,^{4,40} M. Ono,³⁹ V. Onuchin,¹² A. Oskarsson,²⁰ L. Österman,²⁰ I. Otterlund,²⁰ K. Oyama,^{7,38} L. Paffrath,^{3,*} A. P. T. Palounek,¹⁹ V. S. Pantuev,²⁸ V. Papavassiliou,²⁶ S. F. Pate,²⁶ T. Peitzmann,²² A. N. Petridis,¹³ C. Pinkenburg,^{3,27} R. P. Pisani,³ P. Pitukhin,¹² F. Plasil,²⁹ M. Pollack,^{28,36} K. Pope,³⁶ M. L. Purschke,³ I. Ravinovich,⁴² K. F. Read,^{29,36} K. Reygers,²² V. Riabov,^{30,35} Y. Riabov,³⁰ M. Rosati,¹³ A. A. Rose,⁴⁰ S. S. Ryu,⁴³ N. Saito,^{31,32} A. Sakaguchi,¹¹ T. Sakaguchi,^{7,41} H. Sako,³⁹ T. Sakuma,^{31,37} V. Samsonov,³⁰ T. C. Sangster,¹⁸ R. Santo,²² H. D. Sato,^{17,31} S. Sato,³⁹ S. Sawada,¹⁴ B. R. Schlei,¹⁹ Y. Schutz,³⁴ V. Semenov,¹² R. Seto,⁵ T. K. Shea,³ I. Shein,¹² T. -A. Shibata,^{31,37} K. Shigaki,¹⁴ T. Shiina,¹⁹ Y. H. Shin,⁴³ I. G. Sibiriyak,¹⁶ D. Silvermyr,²⁰ K. S. Sim,¹⁵ J. Simon-Gillo,¹⁹ C. P. Singh,⁴ V. Singh,⁴ M. Sivertz,³ A. Soldatov,¹² R. A. Soltz,¹⁸ S. Sorensen,^{29,36} P. W. Stankus,²⁹ N. Starinsky,²¹ P. Steinberg,⁸ E. Stenlund,²⁰ A. Ster,⁴⁴ S. P. Stoll,³ M. Sugioka,^{31,37} T. Sugitate,¹¹ J. P. Sullivan,¹⁹ Y. Sumi,¹¹ Z. Sun,⁶ M. Suzuki,³⁹ E. M. Takagui,³³ A. Taketani,³¹ M. Tamai,⁴¹ K. H. Tanaka,¹⁴ Y. Tanaka,²⁴ E. Taniguchi,^{31,37} M. J. Tannenbaum,³ J. Thomas,²⁸ J. H. Thomas,¹⁸ T. L. Thomas,²⁵ W. Tian,^{6,36} J. Tojo,^{17,31} H. Torii,^{17,31} R. S. Towell,¹⁹ I. Tserruya,⁴² H. Tsuruoka,³⁹ A. A. Tsvetkov,¹⁶ S. K. Tuli,⁴ H. Tydesjö,²⁰ N. Tyurin,¹² T. Ushiroda,²⁴ H. W. van Hecke,¹⁹ C. Velissaris,²⁶ J. Velkovska,²⁸ M. Velkovsky,²⁸ A. A. Vinogradov,¹⁶ M. A. Volkov,¹⁶ A. Vorobyov,³⁰ E. Vznuzdaev,³⁰ H. Wang,⁵ Y. Watanabe,^{31,32} S. N. White,³ C. Witzig,³ F. K. Wohn,¹³ C. L. Woody,³ W. Xie,^{5,42} K. Yagi,³⁹ S. Yokkaichi,³¹ G. R. Young,²⁹ I. E. Yushmanov,¹⁶ W. A. Zajc,⁸ Z. Zhang,²⁸ and S. Zhou⁶

(PHENIX Collaboration)

¹*Institute of Physics, Academia Sinica, Taipei 11529, Taiwan*

²*Bhabha Atomic Research Centre, Bombay 400 085, India*

³*Brookhaven National Laboratory, Upton, NY 11973-5000, USA*

⁴*Department of Physics, Banaras Hindu University, Varanasi 221005, India*

⁵*University of California - Riverside, Riverside, CA 92521, USA*

⁶*China Institute of Atomic Energy (CIAE), Beijing, People's Republic of China*

⁷*Center for Nuclear Study, Graduate School of Science, University of Tokyo, 7-3-1 Hongo, Bunkyo, Tokyo 113-0033, Japan*

⁸*Columbia University, New York, NY 10027 and Nevis Laboratories, Irvington, NY 10533, USA*

⁹*Florida State University, Tallahassee, FL 32306, USA*

¹⁰*Georgia State University, Atlanta, GA 30303, USA*

¹¹*Hiroshima University, Kagamiyama, Higashi-Hiroshima 739-8526, Japan*

- ¹²*Institute for High Energy Physics (IHEP), Protvino, Russia*
¹³*Iowa State University, Ames, IA 50011, USA*
¹⁴*KEK, High Energy Accelerator Research Organization, Tsukuba-shi, Ibaraki-ken 305-0801, Japan*
¹⁵*Korea University, Seoul, 136-701, Korea*
¹⁶*Russian Research Center "Kurchatov Institute", Moscow, Russia*
¹⁷*Kyoto University, Kyoto 606, Japan*
¹⁸*Lawrence Livermore National Laboratory, Livermore, CA 94550, USA*
¹⁹*Los Alamos National Laboratory, Los Alamos, NM 87545, USA*
²⁰*Department of Physics, Lund University, Box 118, SE-221 00 Lund, Sweden*
²¹*McGill University, Montreal, Quebec H3A 2T8, Canada*
²²*Institut für Kernphysik, University of Münster, D-48149 Münster, Germany*
²³*Myongji University, Yongin, Kyonggido 449-728, Korea*
²⁴*Nagasaki Institute of Applied Science, Nagasaki-shi, Nagasaki 851-0193, Japan*
²⁵*University of New Mexico, Albuquerque, NM 87131, USA*
²⁶*New Mexico State University, Las Cruces, NM 88003, USA*
²⁷*Chemistry Department, State University of New York - Stony Brook, Stony Brook, NY 11794, USA*
²⁸*Department of Physics and Astronomy, State University of New York - Stony Brook, Stony Brook, NY 11794, USA*
²⁹*Oak Ridge National Laboratory, Oak Ridge, TN 37831, USA*
³⁰*PNPI, Petersburg Nuclear Physics Institute, Gatchina, Russia*
³¹*RIKEN (The Institute of Physical and Chemical Research), Wako, Saitama 351-0198, JAPAN*
³²*RIKEN BNL Research Center, Brookhaven National Laboratory, Upton, NY 11973-5000, USA*
³³*Universidade de São Paulo, Instituto de Física, Caixa Postal 66318, São Paulo CEP05315-970, Brazil*
³⁴*SUBATECH (Ecole des Mines de Nantes, IN2P3/CNRS, Universite de Nantes) BP 20722 - 44307, Nantes-cedex 3, France*
³⁵*St. Petersburg State Technical University, St. Petersburg, Russia*
³⁶*University of Tennessee, Knoxville, TN 37996, USA*
³⁷*Department of Physics, Tokyo Institute of Technology, Tokyo, 152-8551, Japan*
³⁸*University of Tokyo, Tokyo, Japan*
³⁹*Institute of Physics, University of Tsukuba, Tsukuba, Ibaraki 305, Japan*
⁴⁰*Vanderbilt University, Nashville, TN 37235, USA*
⁴¹*Waseda University, Advanced Research Institute for Science and Engineering, 17 Kikui-cho, Shinjuku-ku, Tokyo 162-0044, Japan*
⁴²*Weizmann Institute, Rehovot 76100, Israel*
⁴³*Yonsei University, IPAP, Seoul 120-749, Korea*
⁴⁴*KFKI Research Institute for Particle and Nuclear Physics (RMKI), Budapest, Hungary[†]*
(November 8, 2018)

Two particle azimuthal correlation functions are presented for charged hadrons produced in Au + Au collisions at RHIC ($\sqrt{s_{NN}} = 130$ GeV). The measurements permit determination of elliptic flow without event-by-event estimation of the reaction plane. The extracted elliptic flow values (v_2) show significant sensitivity to both the collision centrality and the transverse momenta of emitted hadrons, suggesting rapid thermalization and relatively strong velocity fields. When scaled by the eccentricity of the collision zone ε , the scaled elliptic flow shows little or no dependence on centrality for charged hadrons with relatively low p_T . A breakdown of this ε scaling is observed for charged hadrons with $p_T > 1.0$ GeV/c for the most central collisions.

PACS 25.75.Ld

The primary goal of current relativistic heavy ion research is the creation and study of nuclear matter at high energy densities [1–5,7]. Open questions include the detailed properties of such excited matter, as well as the existence of a transition to the quark-gluon plasma (QGP) phase. Such a phase of deconfined quarks and gluons has been predicted to survive for $\approx 3 - 10$ fm/c in Au + Au collisions at the Relativistic Heavy Ion Collider (RHIC) [8], and several experimental probes have been proposed for its possible detection and study [1]. Elliptic flow constitutes an important observable [9–16] because

it is thought to be driven by pressure built up early in the collision, and therefore can reflect conditions existing in the first few fm/c. Elliptic flow leads to an anisotropy in the azimuthal distribution of emitted particles. A Fourier decomposition of this distribution [17,18]

$$\frac{dN}{d(\phi - \Phi_R)} \propto \left(1 + \sum_{n=1}^{\infty} 2v_n \cos(n(\phi - \Phi_R))\right), \quad (0.1)$$

provides a characterization of the elliptic flow via the second Fourier coefficient v_2 . Here, ϕ is the azimuthal angle of an emitted particle and Φ_R is the azimuth of the

reaction plane, defined by the beam direction and the impact parameter vector [19]. The apparent reaction plane is determined from the azimuthal correlations between emitted particles, and its dispersion correction from the azimuthal correlations between two “subevents” [19–21]. An alternative technique for elliptic flow analysis, is the Fourier decomposition of the pair-wise distribution in the azimuthal angle difference ($\Delta\phi = \phi_1 - \phi_2$) between pairs of emitted particles [22–24]:

$$\frac{dN}{d\Delta\phi} \propto \left(1 + \sum_{n=1}^{\infty} 2v_n^2 \cos(n\Delta\phi)\right). \quad (0.2)$$

In this case the magnitude of the elliptic flow is characterized by the square of the second Fourier coefficient in Eq. (0.1), i.e. v_2^2 . These methods of analysis can be taken as equivalent since (i) the correlation between every particle and the reaction plane induces correlations among the particles, and (ii) correlating two subevents amounts to summing two-particle correlations [18]. The results in this letter have several advantages over elliptic flow measurements already performed at the same beam energy by the STAR [5] and PHOBOS [6] collaborations. First, two particle correlations circumvent the need for full azimuthal detector acceptance. Second, it allows the determination of elliptic flow without event-by-event estimation of the reaction plane and the associated corrections for its dispersion. Third, this method can serve to minimize many important systematic uncertainties (detector acceptance, efficiency, etc) which may influence the accuracy of elliptic flow measurements [22,23].

Elliptic flow is predicted and found to be negative for beam energies $\lesssim 4$ AGeV and positive for higher beam energies in Au + Au collisions [9,13–16]. Recent theoretical investigations have made predictions for the centrality dependence of the scaled elliptic flow $A_2 \equiv v_2/\varepsilon$ [25,26] where ε is the eccentricity or initial spatial anisotropy of the “participant” nucleons in the collision zone. The eccentricity ε shows an essentially linear variation with impact parameter b , for $0.2b_{max} \lesssim b \lesssim 0.8b_{max}$ [9] in Au + Au collisions ($b_{max} \approx 14$ fm). For central collisions ($b \lesssim 5 - 6$ fm), it is predicted that higher energy densities are produced and rapid kinetic equilibration in the QGP phase leads to a characteristic rise in A_2 [25,26]. In addition, elliptic flow for high p_T particles has been proposed as an observable sensitive to the energy loss of scattered partons in a QGP phase [27].

The colliding Au beams ($\sqrt{s_{NN}} = 130$ GeV) used in these measurements have been provided by the Relativistic Heavy Ion Collider at Brookhaven National Laboratory (BNL). Charged reaction products were detected in the east and west central arms of the PHENIX detector [2,28]. Each of these arms subtends 90° in azimuth ϕ , and ± 0.35 units of pseudo-rapidity η . The axially symmetric magnetic field of PHENIX (0.5 T) allowed for the tracking of particles with $p_T \geq 200$ MeV/c in the fiducial vol-

ume of both arms. The Drift Chamber (DC) and a layer of Pad Chambers (PC1) located at radii of 2 m and 2.5 m respectively, in each arm, served as the primary tracking detector for these measurements. A second layer of Pad Chambers (PC3), positioned at 5 m in the east arm, was employed to confirm the trajectory of charged particles which traversed both the DC and PC1. The Zero Degree Calorimeters (ZDC), were used in conjunction with the Beam-Beam Counters (BBC) to provide the position of the vertex along the beam direction as well as a trigger for a wide range of centrality selections.

The present data analysis uses two-particle azimuthal correlation functions to measure the distribution of the azimuthal angle difference ($\Delta\phi = \phi_1 - \phi_2$) between pairs of charged hadrons. Following an approach commonly exploited in interferometry studies, a two-particle azimuthal correlation function can be defined as follows [22–24]

$$C(\Delta\phi) = \frac{N_{cor}(\Delta\phi)}{N_{uncor}(\Delta\phi)}, \quad (0.3)$$

where $N_{cor}(\Delta\phi)$ is the observed $\Delta\phi$ distribution for charged particle pairs selected from the same event, and $N_{uncor}(\Delta\phi)$ is the $\Delta\phi$ distribution for particle pairs selected from mixed events. Events were selected with a collision vertex position, $-20 < z < 20$ cm, along the beam axis. Mixed events were obtained by randomly selecting each member of a particle pair from different events having similar multiplicity and vertex position. In order to suppress an over-efficiency in finding two tracks at close angles, hadron pairs within 1 cm of each other in the DC were removed from both the $N_{cor}(\Delta\phi)$ and $N_{uncor}(\Delta\phi)$ distributions. Event centralities were obtained via a series of cuts in the space of BBC versus ZDC analog response [2]; they reflect percentile selections of the total interaction cross section of 6.8 barns [2]. Estimates for the impact-parameter and the eccentricity, $\varepsilon \equiv (\langle y^2 \rangle - \langle x^2 \rangle) / (\langle y^2 \rangle + \langle x^2 \rangle)$ were also made for each of these selections following the model detailed in Ref. [2]. Here, $\langle \dots \rangle$ represents the spatial average (weighted by the density) of participant nucleons over the transverse plane of the collision zone [11]. Systematic uncertainties associated with the determination of ε are estimated to be $\sim 7\%$.

Correlation functions were obtained via two separate methods. In the first, charged hadron pairs were formed by selecting each particle from a common p_T range (fixed- p_T method). In the second hadron pairs were formed by selecting one member from a fixed p_T range and the other from outside this range (assorted- p_T method). Within statistical errors, both methods of analysis yield similar results for the p_T range presented below, as would be expected for a system dominated by collective motion.

An important prerequisite for reliable flow extraction from PHENIX data is to establish whether or not the

$\sim 180^\circ$ azimuthal coverage of the detector results in significant distortions to the correlation function. To this end, detailed simulations of the detector response, acceptance and efficiency, have been performed for simulated data incorporating specific amounts of flow (parameterized by v_2). The results from these simulations indicated no significant distortion to the correlation functions due to the PHENIX acceptance. On the other hand, small distortions to the correlation function (for $\Delta\phi \lesssim 25^\circ$) as well as an incomplete recovery of v_2 could be attributed to background contributions.

These background contributions principally affect the extraction of v_2 from the correlation function in two ways. The distortion to the correlation function at small relative angle introduces a small systematic distortion when fit with a Fourier function [c.f. Eq. (0.2)]. A good representation of the data was obtained with the fit function $C(\Delta\phi) = \lambda \cdot \exp(-0.5(\Delta\phi/\sigma)^2) + a_1 \cdot (1 + 2v_2^2 \cos(2\Delta\phi))$, where the Gaussian term is used to characterize the background distortion at small angles. In addition, there is an isotropic background of false tracks which are predominantly misidentified as high p_T particles. These contributions can be efficiently suppressed in the east central arm of PHENIX, by requiring a relatively stringent association between tracks found in the DC and their associated hits in PC3. Using such a procedure, the fraction of background tracks has been evaluated as a function of p_T and used to correct v_2 . Corrections range from $\sim 10\%$ at low p_T to $\sim 25\%$ at 2 GeV/c with a systematic uncertainty of 5%. The current analysis is restricted to the range $0.3 < p_t \leq 2.5$ GeV/c to maintain this relatively small systematic uncertainty.

Figures 1a - d show representative $\Delta\phi$ correlation functions obtained for charged hadrons detected in the pseudo-rapidity range $-0.35 < \eta < 0.35$. Correlation functions for relatively central events (centrality = 20 - 25%, $b \sim 7.0$ fm) are shown for hadrons with $0.3 < p_T < 2.5$ GeV/c and $0.5 < p_T < 2.5$ GeV/c in Figs. 1a and c respectively. The same p_T selections have been made for the correlation functions shown in Figs. 1b and d but for more peripheral collisions (centrality = 40 - 45%, $b \sim 9.6$ fm) as indicated. Figs. 1a - d show a clear anisotropic pattern which is essentially symmetric about $\Delta\phi = 90^\circ$. There is also a visible increase of this anisotropy with increasing impact parameter and p_T . These trends are all consistent with those expected for in-plane elliptic flow [10,11,13,20].

The magnitude of elliptic flow and the mechanism for its development, can be shown to be related to (a) the geometry of the collision zone, (b) the initial baryon and energy density developed in this zone, and (c) the detailed nature of the equation of state for the created nuclear matter [9–13,25]. Since differential flow measurements can serve to provide important insights for disentangling these separate aspects [10–13,25], we show the results of such measurements in Figs. 2 and 3. Fig. 2

shows v_2 as a function of centrality for several p_T selections; $0.40 < p_T < 0.60$ (diamonds), $0.60 < p_T < 1.00$ (squares), and $1.0 < p_T < 2.5$ (circles) GeV/c respectively. Fig. 3 compares the differential flow $v_2(p_T)$, for several centralities as indicated.

Figs. 2 and 3 both show relatively large differential flow values which increase with increasing impact parameter and the p_T of emitted hadrons. The separate effects of spatial asymmetry and the response of the collision zone to the generated pressure are also evident in Fig. 3. That is, v_2 not only increases with increasing impact parameter for a fixed p_T , but also increases with increasing p_T for a fixed centrality selection. Trivially, the magnitude of flow should go to zero for very small and very large impact parameters. Similarly, its magnitude can be expected to be zero for $p_T = 0$. It is interesting that Fig. 3 indicates an essentially linear rise of v_2 with p_T for each of the centrality selections presented. Such a trend can not be accounted for via simple geometric considerations alone [29]. However, it is compatible with model calculations which assume a strong transverse velocity field [29]. This suggests the presence of strong dynamically driven transverse flow at RHIC. The magnitude and trends for v_2 shown in Figs. 2 and 3 are consistent with other elliptic flow measurements at RHIC [5,6].

Figure 4 aims to disentangle the geometric and dynamical (p_T) contributions to the elliptic flow over a broad range of centralities or energy densities. To do this, we plot A_2 as a function of centrality to obtain the dynamical contributions [25,26]. This evaluation is performed for two p_T selections ($0.40 < p_T < 0.60$ and $1.0 < p_T < 2.5$ GeV/c) which give rise to relatively low and high p_T values respectively. The underlying idea is that this ratio should remove the geometric dependence of v_2 , while the p_T selections may provide greater sensitivity to different time scales and energy densities associated with the expanding system.

Figure 4 shows an increase in the magnitude of A_2 with increasing p_T . This increase can be attributed to the dynamical response of the created system, resulting from the generated pressure gradients. For hadrons of $0.4 < p_T < 0.6$ the observed centrality dependence of A_2 is compatible with ε scaling. However, a breakdown of this scaling is observed for hadrons with $1.0 < p_T < 2.5$. Such a trend may point to a change in the particle production mechanism or the possibility that pressures larger than those predicted by current hydrodynamic calculations [10,11] are being produced in the most central collisions at RHIC. It is also interesting to note that the species composition of the charged particle spectra changes dramatically between the two p_T ranges used in Fig. 4 [30].

To summarize, we have measured two-particle azimuthal correlation functions for charged hadrons produced in Au + Au collisions at RHIC ($\sqrt{s_{NN}} = 130$ GeV). The integral, differential and scaled elliptic flow values

extracted from these measurements indicate strong sensitivity to the collision centrality and the transverse momenta of emitted hadrons. The centrality dependence of v_2 suggests that the high-energy-density nuclear matter created at RHIC, efficiently translates the initial spatial asymmetry into a similar asymmetry in momentum space. The p_T dependence is consistent with the development of strong transverse velocity fields in the collision zone. The centrality dependence of A_2 for hadrons in the range $0.4 < p_T < 0.6$ is compatible with ε scaling. However, a breakdown of this scaling is observed for hadrons with $1.0 < p_T < 2.5$. Such a trend could result from a number of effects, the most intriguing of which is a possible change in the equation of state [25,26]. Additional experimental signatures and model calculations will undoubtedly be necessary to test the detailed implications of these results. Nevertheless, the results presented here clearly show that two particle azimuthal correlation measurements provide an important probe for the high-energy-density nuclear matter created at RHIC.

We thank the staff of the Collider-Accelerator and Physics Departments at BNL for their vital contributions. We acknowledge support from the Department of Energy and NSF (U.S.A.), MEXT and JSPS (Japan), RAS, RMAE, and RMS (Russia), BMBF, DAAD, and AvH (Germany), VR and KAW (Sweden), MIST and NSERC (Canada), CNPq and FAPESP (Brazil), IN2P3/CNRS (France), DAE and DST (India), KRF and CHEP (Korea), the U.S. CRDF for the FSU, and the US-Israel BSF.

[1] S. Bass *et al.*, Nucl.Phys. **A661** 205 (1999).
[2] K. Adcox *et al.*, Phys. Rev. Lett. **86**, 3500 (2001).
[3] K. Adcox *et al.*, Phys. Rev. Lett. **87**, 52301 (2001).
[4] W. Zajc (PHENIX Collaboration) Nucl. Phys. **A698**, 39c (2002).
[5] K.H. Ackermann *et al.* Phys. Rev. Lett. **86** 402 (2001).
[6] I. Park (PHOBOS Collaboration) Nucl. Phys. **A698**, 564c (2002).
[7] B.B. Back *et al.*, Phys. Rev. Lett. **85** 3100 (2000).
[8] B. Zhang, M. Gyulassy, and C.M. Ko, Phys. Lett. **B 455** 45 (1999).
[9] J.-Y. Ollitrault, Phys. Rev. **D 46** (1992) 229.
[10] D. Teaney, J. Lauret, and E.V. Shuryak, Phys. Rev. Lett. **86**, 4783 (2001).
[11] P. F. Kolb *et al.*, hep-ph/0103234.
[12] E. E. Zabrodin *et al.*, nucl-th/0104054.
[13] P. Danielewicz *et al.*, Phys. Rev. Lett. **81**, 2438 (1998).
[14] J. Barrette *et al.*, Phys. Rev. C **55**, 1420 (1997).
[15] H. Appelshäuser *et al.*, Phys. Rev. Lett. **80**, 4136 (1998).
[16] C. Pinkenburg *et al.*, Phys. Rev. Lett. **83**, 1295 (1999).
[17] H. H. Gutbrod *et al.*, Phys. Rev. C **56**, **42**, 640 (1990).
[18] N. Borghini *et al.*, nucl-th/0105040.

[19] P. Danielewicz and G. Odyniec, Phys. Lett. **157B**, 146 (1985).
[20] J.-Y. Ollitrault, Nucl. Phys. A638 195c-206c (1998).
[21] A. M. Poskanzer *et al.*, Phys. Rev. C **58**, 1671, (1988).
[22] S. Wang *et al.*, Phys. Rev. C **44**, 1091 (1991).
[23] R. Lacey *et al.*, Phys. Rev. Lett. **70**, 1224 (1993).
[24] R. Lacey (PHENIX Collaboration), Nucl. Phys. **A698**, 559c (2002).
[25] H. Sorge Phys. Rev. Lett. **82**, 2048 (1999).
[26] H. Heiselberg, A. Levy Phys. Rev. C **59** 2716, (1999).
[27] M. Gyulassy, I. Vitev, X. N. Wang, Phys. Rev. **86**, 2537 (2000).
[28] D.P. Morrison (PHENIX Collaboration), Nucl. Phys. **A638**, 565c (1998); N. Saito (PHENIX Collaboration), *ibid* p. 575c.
[29] P. Huovinen nucl-th/0104020.
[30] K. Adcox *et. al*, nucl-ex/0112006 (sub. Phys. Rev. Lett.)

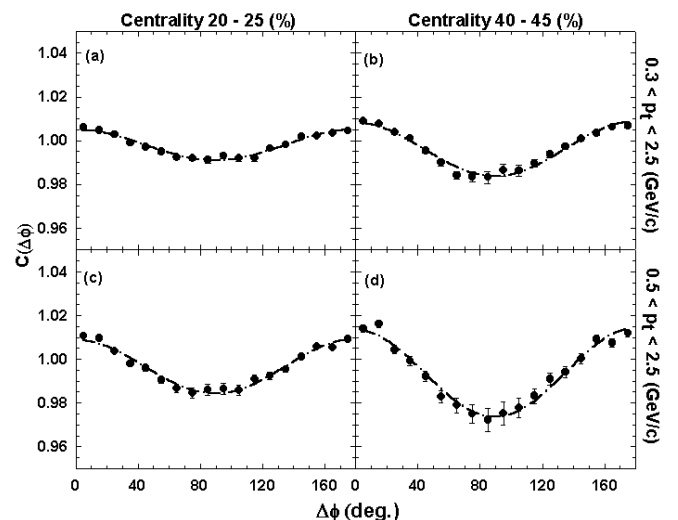


FIG. 1. Azimuthal correlation functions for charged hadrons as a function of centrality and p_T selection. The solid curves represent Fourier fits following Eq. (2). Error bars are statistical only.

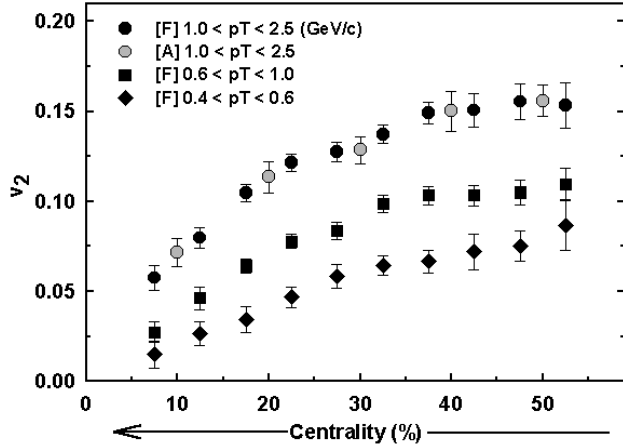


FIG. 2. v_2 vs. centrality for several p_T selections. [F] and [A] indicate results obtained with the fixed- p_T and assorted- p_T methods respectively. Systematic errors are estimated to be $\sim 5\%$; they are dominated by the normalization of the correction function for real tracks. For the centrality range 0-5% the data points are statistically uncertain and the points are omitted.

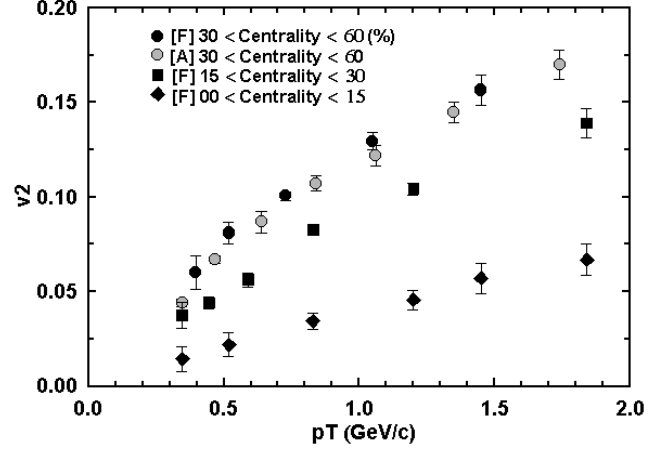


FIG. 3. v_2 vs p_T for several centrality selections. [F] and [A] follow the notation Fig. 2. Systematic errors are estimated to be $\sim 5\%$.

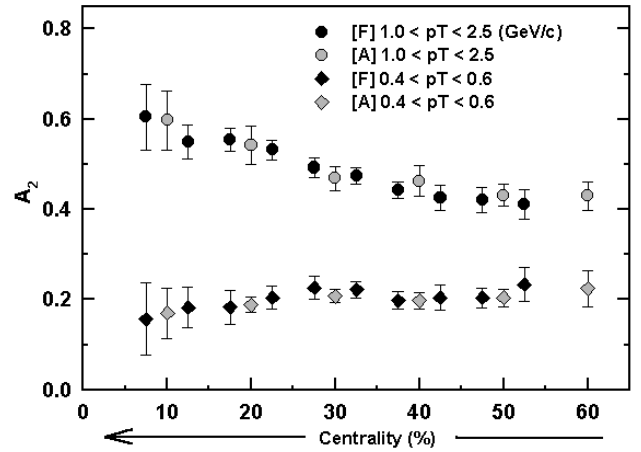


FIG. 4. The centrality dependence of A_2 for two different p_T selections. [F] and [A] follow the notation in Fig. 2. Systematic errors are estimated to be $\sim 10\%$, dominated by the normalization of the correction function and the model determination of ϵ .